Journal: Physics and Chemistry of the Earth
MS No.: G-10-011
First author: Elósegui

An Experiment for Estimation of the Spatial and Temporal Variations of Water Vapor using GPS data

P. Elósegui[1,2], A. Rius[1], J. L. Davis[2], G. Ruffini[1], S.J. Keihm[3], B. Bürki[4], and L.P. Kruse[4]

[1]Institut d'Estudis Espacials de Catalunya, Unidad de Investigación del CSIC, E-08034-Barcelona, Spain
[2]Harvard-Smithsonian Center for Astrophysics, Cambridge, MA 02138, USA
[3]Jet Propulsion Laboratory, Pasadena, California, 91109, USA
[4]ETH-Hoenggerberg, CH-8093 Zurich, Switzerland

Received 21 April 1997 – Accepted 14 November 1997

Abstract. We have investigated the spatial and temporal variations of atmospheric water vapor using estimates of differential zenith wet delay. These estimates were obtained from an experiment involving Global Positioning System (GPS) receivers at five sites near Madrid, Spain. Data were acquired for 14 consecutive days in December 1996. The intersite horizontal separation varied from 5 km to 50 km (with a maximum altitude difference between sites of 400 m). The sampling rate for the GPS observations was 30 s, except for 2 days during which we used a sampling rate of 10 s. The GPS data were used to estimate relative zenith wet delays. One of the GPS receiving systems was colocated with a continuously operating dual-channel Water Vapor Radiometer (WVR). During the entire experiment the WVR obtained observations from a fixed pattern of directions intended to "map" the water-vapor distribution. We have found that these estimates of differential zenith wet delay are highly correlated with the altitude of the site and that the wet refractivity, on average, followed an exponential distribution with an assumed scale height of 1.5 km. We present results from this experiment, including the high degrees of correlation observed both in the spatial and temporal domains once the estimates of differential zenith wet delay were normalized after this exponential law.

1 Introduction

A radio signal with origin in a distant, extra-terrestrial source (say, for instance, a GPS satellite) and received by a ground-based antenna will be refracted by the neutral atmosphere of the Earth. The refraction effects will cause an extra time, or propagation delay, for the signal to reach the antenna relative to the time it would take were the atmosphere be replaced by vacuum. Within the neutral atmosphere, the propagation of radio waves is mostly affected by the troposphere. In the troposphere, water vapor plays a particularly important role in radio propagation and in a variety of atmospheric processes.

The component of the neutral atmosphere in hydrostatic equilibrium, primarily nitrogen and oxygen, can be quite accurately estimated simply by measuring the barometric pressure at the surface (Davis et al., 1985). The total column density of water vapor, however, cannot be accurately sensed from surface meteorological measurements because it is very poorly mixed in the atmosphere and presents large spatial and temporal variability. At sea level in the local zenith direction, the additional delay that the signal experiences due to the hydrostatic component of the troposphere is ∼2300 mm. The corresponding nominal delay caused by the water vapor, called "wet delay," is ∼100 mm, with extreme values of about 400 mm in the tropics.

It is generally thought that uncertainties in the water vapor content are a fundamental limitation to the accuracy of space geodetic radio techniques such as GPS and very-long baseline interferometry (VLBI). Radio observations carried out with these techniques can be used, alternatively, to probe the characteristics of the propagation media. In order to account for the atmospheric propagation effects a combination of modelling and estimation is usually employed. Currently, water vapor variations are commonly modeled as a random walk stochastic process and are estimated by employing some kind of filtering analysis (Herring et al., 1990; Lichten, 1990). The accuracy of these wet delay estimates are of the order of a few mm.

Another method for estimation of the wet delay is based on WVRs (Resch, 1984; Elgered et al., 1991). WVRs can determine wet delays (with a precision of 1–3 mm and an accuracy of about 5–10 mm) from measurements of the brightness temperature at frequencies near the 22.2-GHz water vapor resonance.

This paper describes our investigations leading to the

Correspondence to: P. Elósegui

Table 1. Instrumentation

Site	Alt.	GPS		WVR	Radiosonde
	(m)	Rec.†	Ant.‡		
BARA	633				Barajas
IGNE	767	TR4S	TRGP		
VILA	648	TR4S	TRGP	ETH	
VALD	845	TR4S	TRGP		
ESCO	1078	TR4S	TRGP	ETH	
ROBL	829	TR4S	TRGP	ETH	
VILL	648	RS81	DMT		
MADR	829	RS80	DMT	JPL	

† TR4S, Trimble 4000SSE; RS81, Rogue SNR-8000; RS80, Rogue SNR-8100
‡ TRGP, Trimble geodetic L1/L2 with ground plane; DMT, Dorne Margolin T

study of the spatial and temporal variations of atmospheric water vapor as obtained from a GPS experiment carried out with that purpose. In the following sections, we will first describe the experiment and the data used for the analysis and then present and discuss (in the form of spatial and temporal plots) the results.

2 Experiment Description

We acquired data with GPS receivers and WVRs in the Madrid area, Spain, on December 2–15, 1996. Figure 1 shows the geographical location of the sites involved in this experiment. We deployed five Trimble geodetic GPS receiver systems, with intersite separations of between 5 km and 50 km. Two of these antennas were installed each within 5 m of two of the permanent sites of the International GPS Service for Geodynamics (IGS). These two IGS sites, MADR and VILL, employ Rogue receiver systems. The observations consisted of samples, from 6 to 8 satellites, of undifferenced dual-frequency carrier-phase and pseudo-range measurements obtained every 30 s for all but for 2 days, during which we used a sampling rate of 10 s instead.

In addition to the permanent JPL D-series WV radiometer (Keihm, 1991) located next to the IGS site MADR at the INTA-NASA Deep Space Network Complex, three dual-channel ETH WVRs (Bürki et al., 1992) were simultaneously operated at three of the sites of this regional GPS network. Unfortunately, during the time of this experiment the weather was unusually bad, with many days of continuous heavy rains. During the entire experiment, the WVRs acquired observations from a fixed pattern of directions intended to "map" the water-vapor distribution. The estimates of zenith wet delays obtained from the JPL radiometer for this time period present extremely high scatter due to the rain, with only a few intervals (see Fig. 2) not being contaminated by heavy cloud cover and/or by the wetting of the radiometer window by rainfall. The estimated accuracy of the absolute zenith wet delays (not shown) for these intervals is about 10 mm, with a precision of about 2 mm for

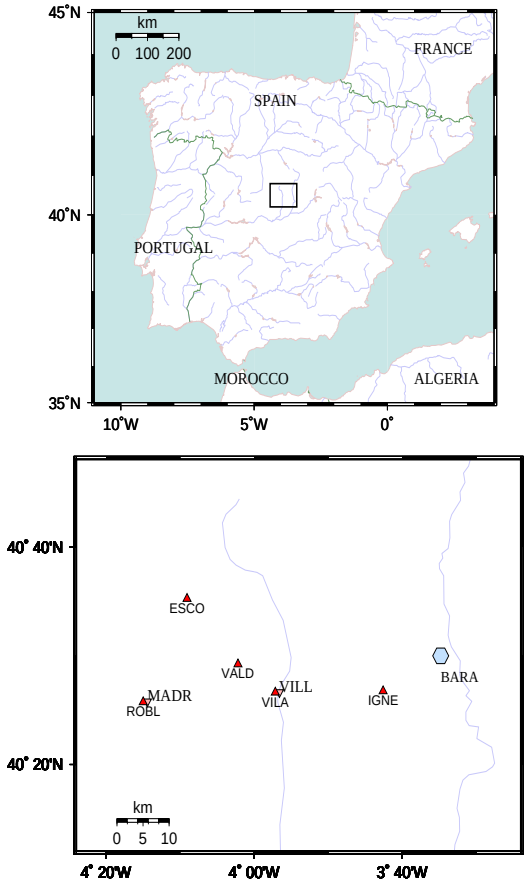

Fig. 1. Box in map of Spain (top) positions the regional network (bottom), which shows the location of the sites involved in this experiment. The GPS stations (triangles), the two IGS sites (inverted triangles), and the radiosonde launch site (hexagon) are labeled after the four-character codes defined in Table 1.

contiguous data. For calibration purposes, one the ETH radiometers was installed side-by-side with the JPL radiometer and the GPS receiver. However, the three ETH radiometers suffered from the same environmental problems. Because of this added difficulty in deriving zenith wet delays from the radiometers, the comparison between the two types of WVRs and of them with the GPS data will not be discussed in this paper.

Radiosonde data were also acquired twice per day, at around 0 and 12 UTC, during the time of these observations at the Madrid-Barajas airport, located at about 20 km to the east of IGNE, the easternmost site of our GPS network (see Fig. 1). These data consist of height profiles of the climatic (pressure, temperature, and relative humidity) state of the atmosphere. We are currently studying the use of these data as an external check for the model used to normalize with altitude the estimates of differential zenith wet delay (see Sect. 4), which will be reported in a future paper.

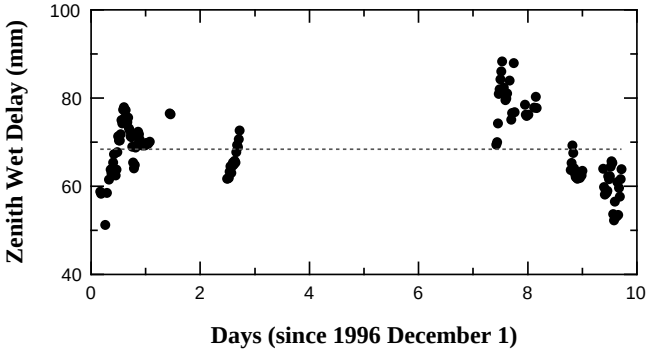

Fig. 2. Estimates of the wet zenith delay from the JPL WVR. The dotted line is the mean value, 69 mm.

3 Data Analysis

We used a standard strategy to process the GPS data using the software package GIPSY-OASIS II (v.4) (Webb and Zumberge, 1993). Using the data from each day (starting at 0 UTC), together with precise orbits and consistent earth-rotation parameters both procured from IGS, we formed the carrier phase (LC) and pseudo-range ionosphere-free linear combination and estimated the three components of position of the five Trimble sites, carrier phase ambiguities, satellite and station clocks, and differential atmospheric zenith delays relative to ROBL, which was not estimated. The root-mean-square (RMS) postfit LC phase residual was typically ∼4–5 mm.

We modeled the atmospheric delays, τ_a, as the sum of a constant term over the length of the experiment and a time-varying term, which represented the hydrostatic and the wet components, respectively:

$$\tau_a(\epsilon) = \tau_h^z m_h(\epsilon) + \tau_w^z m_w(\epsilon) \quad (1)$$

where ϵ is the observation elevation angle, τ_h^z and τ_w^z are the zenith delays for the hydrostatic and wet atmosphere components, and m_h and m_w are the hydrostatic and wet mapping functions, which describe the elevation angle dependence of the zenith atmospheric delay. We used Niell (1996) hydrostatic and wet mapping functions.

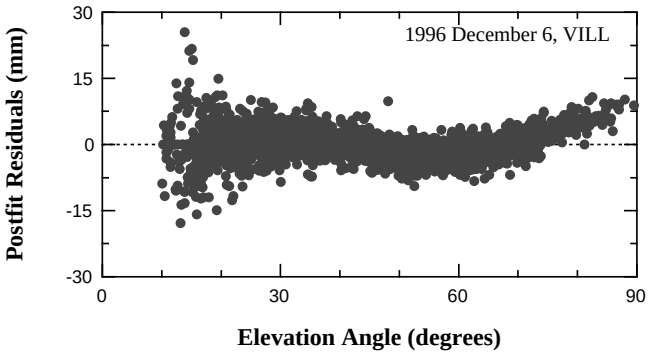

Fig. 3. Postfit LC phase residuals for the 5 m long VILA-VILL baseline, plotted as a function of elevation angle.

GIPSY computes a priori values for the nominal zenith hydrostatic delays using an exponential law based on the altitude of the site above the ellipsoid. We used a nominal sea level pressure of 1013.25 mbar, a scale height of 8.6 km, and a pressure-to-delay conversion factor of 0.002277 m mbar^{-1}. The value for the scale height was calculated by comparing the pressure ratios from the readings of the barometers that we installed at the WVR sites and using this same exponential law for pressure variations. The equivalent zenith hydrostatic delays were also computed from surface pressure measurements obtained from precise (∼0.3 mbar) barometric readings at the MADR site. An average, over the entire time period of the experiment, pressure of 924.2 mbar was measured at this site, with a (peak-to-peak) pressure difference of 23.9 mbar. For this site, the pressure calculated using the exponential model is 920.1 mbar. Therefore, the difference between the nominal and average pressures is negligible when compared to the actual pressure variations recorded during the 14-day period. The maximum zenith hydrostatic delay error for not correcting for both pressure differences and pressure variations amounts to 2.8 mm, which is smaller than the uncertainties associated with estimates of the differential zenith wet delays.

Zenith wet delays were modeled as a loosely constrained random walk stochastic process (process noise $\sigma = 0.17$ mm s$^{-1/2}$) and its values were estimated at 300 s intervals. Differential atmospheric wet delays, $\Delta\tau_w$, were estimated as the difference between the wet delays at given site, τ_w^i $(i = 1, 4)$, relative to that of a reference site, τ_w^{ref}. Short baselines are mainly sensitive to the differences between zenith wet delays, and not to their absolute values, because the elevation angles for a given satellite at a given epoch from the two ends of the baseline are very similar. In other words, $m_w(\epsilon^i) \simeq m_w(\epsilon^{ref})$ as the difference between ϵ^i and ϵ^{ref} gets smaller (and the same is of course true for m_h). Then:

$$\Delta\tau_w(\epsilon^i, \epsilon^{ref}) \simeq (\tau_w^{z_i} - \tau_w^{z_{ref}}) m_w(\epsilon) = \Delta\tau_w^z m_w(\epsilon) \quad (2)$$

where $\Delta\tau_w$ is the relative zenith wet delay. The maximum elevation angle difference for the longest baseline in our network (46 km) is $\lesssim 1^\circ$ and, therefore, we estimated relative, and not absolute, zenith wet delays.

Data from the two Rogue systems have not been included in these solutions yet for two reasons, both related to phase-calibration errors due to receiving GPS antennas. The first error is associated with scattering (multipath) from the monument on which the antenna is situated (Elósegui et al., 1995). This error is mainly elevation-angle dependent and has been shown to induce systematic errors in estimates of all parameters, and of our particular concern here, of zenith wet delays (Elósegui et al., 1994). Such errors will virtually cancel only if identical monuments are used and the elevation angle difference between antennas is negligible

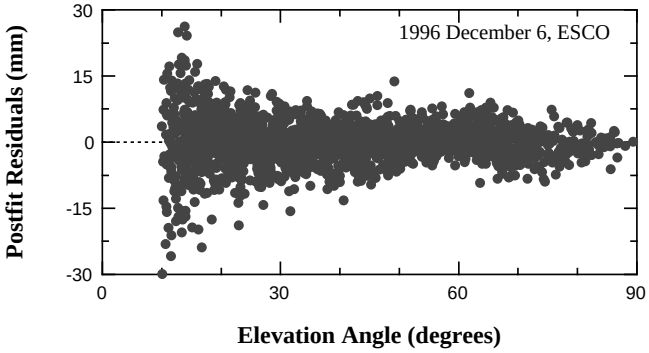

Fig. 4. Postfit phase residuals for the 23 km long ESCO-VILA baseline, plotted as a function of elevation angle.

(Jaldehag et al., 1996). The VILL antenna is mounted on a concrete and metal pillar, which are known to present significant scattering errors. The MADR antenna is mounted on a piece of cast iron. The second error is associated with the phase pattern of the receiving antenna itself. Antenna phase patterns that are not isotropic (all GPS antennas are anisotropic to some degree; see, e.g., Schupler et al. (1994)) cause variations of the position of the phase center with signal direction, which, in turn, introduce systematic errors in estimates of atmospheric delays. This error, for the type of antennas most commonly used in geodetic studies, is mainly, but not exclusively, elevation-angle dependent. As in the previous case, such errors will cancel out if identical antennas are used, so that the variations are similar for all of them, and the elevation angle difference between antennas is small, as it is the case in this experiment. The postfit LC residuals for two different baselines are used here to illustrate the combined presence of these types of errors. First, Fig. 3 clearly indicates a systematic elevation-angle dependent error; the baseline VILL-VILA is 5 m long and VILA was mounted on a wooden tripod. And second, there is not (statistical) indication of such error in Fig. 4, obtained from the 23 km long ESCO-VILA baseline; the two antenna were each mounted on an identical wooden tripod. We are currently testing the effects of using a priori antenna phase-center models on estimates of zenith wet delays, the results of which will be reported elsewhere.

4 Results and Discussion

4.1 Time Series

Figure 5 shows estimates of the differential zenith wet delays, relative to the estimates at the ROBL site, at four sites in the network for the entire 14-day period of the experiment. In this figure, there can readily be identified some features that are common to all sites (e.g., the peak through midnight of December 4–5) which are a sign of some degree of correlation in the water vapor content over the spatial scales sampled by this network.

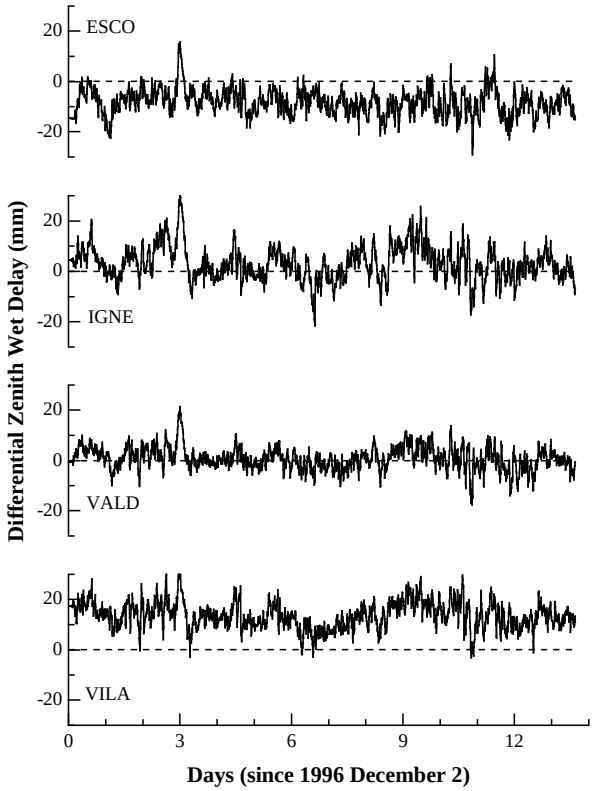

Fig. 5. GPS estimates of the differential wet zenith delays.

We will postpone the discussion of this and other selected features of this time series to the next section. For now, we will turn our attention to another distinctive aspect present in the time series. Examination of Fig. 5 immediately reveals a dependence of the differential zenith wet delay with the altitude of the site relative to that of the reference site. Site altitudes for all five sites are given in column 2 of Table 1. The overall negative differential zenith wet delays at ESCO, the positive at IGNE and VILA, and the absence of almost any at VALD are in agreement with the altitudes of the sites being higher, lower, and similar to that of ROBL, respectively. The average values of these zenith wet delays are (ESCO, IGNE, VILA, VALD): –8.3, 3.1, 13.6, and 0.7 mm. This dependence is due to a scaling on the amount of integrated water vapor with altitude. Because the effect swamps the estimates of differential zenith wet delay, we want to correct for this dependence to enhance the water vapor signal and be able to better focus on the small details. To correct for ("normalize") this height factor, we will assume an exponential law for the water vapor refractivity (Davis et al., 1993). We will assume that this law can be used to represent an "average" refractivity profile:

$$N(z) = N_s\, e^{-z/H} \tag{3}$$

where N is the wet refractivity, z is the altitude, N_s is the wet surface refractivity, and H is the water vapor scale height, which is usually found to be 1–2 km. The

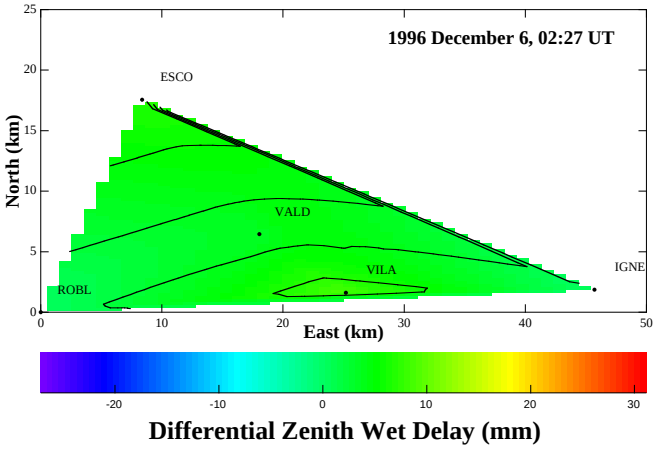

Fig. 6. Spatial distribution of normalized differential zenith wet delays at 02:27 UT on December 6, 1996.

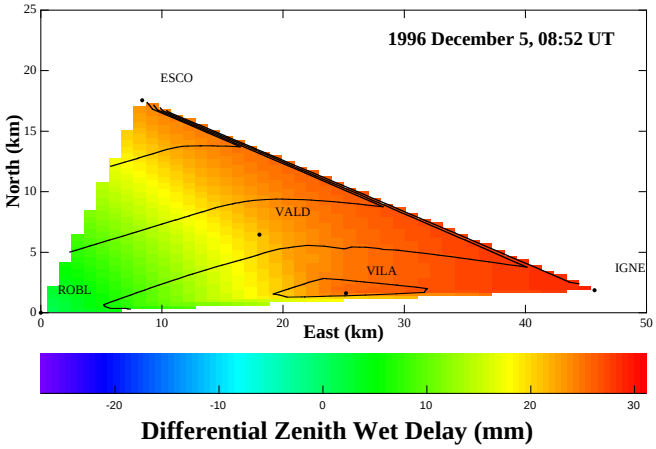

Fig. 7. Spatial distribution of normalized differential zenith wet delays at 08:52 UT on December 5, 1996.

zenith wet delay at sea level, τ_w^{sl}, can be obtained by the integration of Eq. (3):

$$\tau_w^{sl} = \int_0^\infty 10^{-6} N(z) dz = 10^{-6} N_s H \tag{4}$$

The zenith wet delay, τ^i, for a site i at an altitude z_i can then be expressed as a function of τ_w^{sl} as:

$$\tau_w^{z_i} = \int_{z_i}^\infty 10^{-6} N(z) dz = \tau_w^{sl}\, e^{-z_i/H} \tag{5}$$

and using Eq. (5) for two different altitudes, one being that of the reference site, we obtain an expression for normalizing the differential zenith wet delay with altitude:

$$\tau_w^{z_i} - \tau_w^{z_{ref}} = \tau_w^{z_{ref}} \left[e^{-(z_i - z_{ref})/H} - 1 \right] \tag{6}$$

From the estimates of zenith wet delay in Fig. 2, the average value for $\tau_w^{z_{ref}}$ is 69 mm, with the largest deviation being 20 mm. For a scale height of 1.5 km, the resultant normalization constants for the four sites (ESCO, IGNE, VILA, VALD) are: –10.5, 2.9, 8.9, and –0.7 mm. We applied these corrections to the time series shown in Fig. 5. The average values of the differential zenith wet delay for the same four sites and order are now, after normalization: 2.2, 0.2, 4.7, and 1.4 mm. To gain some insight into the variations of water vapor over the network during the time period of our experiment, we now turn onto a pictorial representation, for several time instances, of the distribution of normalized differential zenith wet delay, hereafter referred to as "ndzwd".

4.2 Temporal snapshots of the spatial distribution of ndzwd

Figure 6 shows the spatial distribution of ndzwd (in mm) at 02:27 UT on December 6, 1996 over the entire area of our network. The solid dots in the figure represent the location of the GPS sites relative to that of ROBL, the reference site (see Fig. 1 for geographical coordinates), and the contours depict the generalized topography of the region (contours are in steps of 100 m; see Table 1 for site altitudes). We used a 2-dimensional linear interpolator/smoother to obtain ndzwd at locations other than those where it was estimated. From Fig. 6, the spatial distribution of ndzwd is very uniform, with a maximum variation of about 5 mm. The following two conclusions can be drawn from the fact that this spatial uniformity in the distribution of ndzwd has been found to be, in addition, the most common one throughout the entire 14-day period: (1) the exponential law assumed for the water vapor refractivity does successfully represent the wet refractivity profile over this area to within 5–10 mm; (2) the water vapor content is highly correlated both in the spatial ($\lesssim$50 km) and temporal (from 300 s to 14 days) domains, at least during this particular period.

Departures from this uniformity would indicate deviations from this average atmospheric conditions and would simultaneously be accompanied by space decorrelation, time decorrelation, or both, in the water vapor content. We have had several instances when this behavior has been encountered, two of which are presented in the next two figures. Figure 7 illustrates a case when the distribution of ndzwd over the east area of the network was about 25–30 mm higher than that of ROBL. This "anomalous" increase of ndzwd lasted for about 4 hr, started at ESCO, which is the highest-northernmost site in the network, quickly traveled towards the south-east reaching first VALD, then VILA, and finally IGNE, following the altitude gradient and an east-west trend, reached its maximum at around 08:52 UT on December 5, 1996, which is the time of the snapshot presented in Fig. 7, and then gradually disappeared through the east.

Figure 8 is meant to illustrate a case of a highly variable (over a ∼2-day period), localized minimum in the distribution of ndzwd. From about 15:00 UT on De-

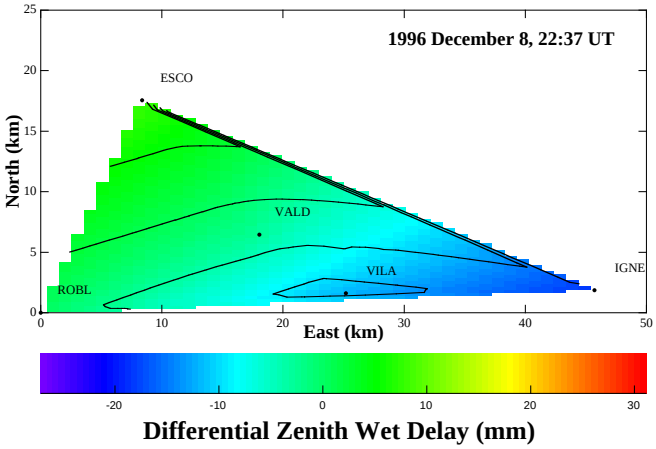

Fig. 8. Spatial distribution of normalized differential zenith wet delays at 22:37 UT on December 8, 1996.

cember 8, 1996, through 04:00 UT on December 10, 1996, the ndzwd followed a pattern of intermittent sudden minima (each lasting for about 1–2 hr) mainly at IGNE, somewhat less at VILA, and significantly less at VALD and ESCO. Figure 8 shows the state of the atmosphere at 22:37 UT on December 8, 1996, with a minimum of about –20 mm localized at IGNE and extending towards VILA. A movie showing estimates of ndzwd for the entire network and time period can be viewed at http://cfageod4.harvard.edu/mad_ndzwd.html.

5 Conclusions

We have studied the spatial and temporal variations of water vapor in the atmosphere by using estimates of differential zenith wet delays derived, at 300 s intervals, from GPS data. These data were acquired during a 14-day period, in December 1996, at five sites near Madrid, in a network of maximum intersite separation of about 50 km. We found that these estimates of differential zenith wet delay are highly correlated with the altitude of the site. Even though the water vapor is not well mixed in the atmosphere, we found that, on average (for at least the 14-day period studied), the wet refractivity followed an exponential distribution with an assumed scale height of 1.5 km. High degrees of correlation both in the spatial and temporal domains were observed once the estimates of differential zenith wet delay were normalized after this exponential law.

Acknowledgements. This work was supported by Spanish Climate CICYT grant CLI95-1781, EC grant WAVEFRONT PL-952007, NASA grant NAG5-538, and the Smithsonian Institution. We gratefully acknowledge use of the facilities of the ESA Satellite Tracking Station in Villafranca del Castillo, the INTA-NASA Complex in Robledo de Chavela, the Patrimonio Nacional and the Agustinos Community of the Monastery of San Lorenzo del Escorial, and of Christian Longhi's private home in Valdemorillo, which were made available to us. The Spanish IGN loaned and operated the GPS receivers. Figure 1 was created with the GMT software.

References

Bürki, B., Cocard, M., Geiger, A., Gyger, R., and Kahle, H.-G., Development of a portable dual frequency microwave water vapor radiometer for geodetic applications, *Refraction of transatmospheric signals in geodesy, Proc. of the Symposium, Netherlands Geodetic Commission, Publications on Geodesy, New Series No. 36*, 129–133, 1992.

Davis, J. L., Herring, T. A., Shapiro, I. I., Rogers, A. E. E., and Elgered, G., Geodesy by radio interferometry: Effects of atmospheric modeling errors on estimates of baseline length, *Radio Science*, *20*, 1593–1607, 1985.

Davis, J. L., Elgered, G., Niell, A. E., and Kuehn, C. E., Ground-based measurements of gradients in the "wet" radio refractivity of air, *Radio Science*, *28*, 1003–1018, 1993.

Elgered, G., Davis, J. L., Herring, T. A., and Shapiro, I. I., Geodesy by radio interferometry: Water vapor radiometry for estimation of the wet delay, *J. Geophys. Res.*, *96*, 6541–6555, 1991.

Elósegui P., Davis, J. L., Shapiro I. I., Jaldehag, R. T. K., Johansson, J. M., and Niell, A. E., Effects of signal multipath on GPS estimates of the atmospheric propagation delay (abstract), *Eos Trans. AGU*, *75*, 173, 1994.

Elósegui P., Davis, J. L., Jaldehag, R. T. K., Johansson, J. M., Niell, A. E., and Shapiro I. I., Geodesy using the Global Positioning System: The effects of signal scattering on estimates of site position, *J. Geophys. Res.*, *100*, 9921–9934, 1995.

Jaldehag, R. T. K., Johansson, J. M., Rönnäng B. O., Elósegui P., Davis, J. L., and Shapiro I. I., Geodesy using the Swedish permanent GPS network: Effects of signal scattering on estimates of relative site positions, *J. Geophys. Res.*, *101*, 17,841–17,860, 1996.

Keihm, S. J., Water vapor radiometer comparison experiment: Platteville, Colorado, March 1-14, 1991, *JPL Publ.*, *D-8898*, 1991.

Janssen, M. A., A new instrument for the determination of radio path delay variations due to atmospheric water vapor, *IEEE Trans. Geosci. Remote Sens.*, *GE-23*, 485–490, 1985.

Herring, T. A., Davis, J. L., and Shapiro, I. I., Geodesy by radio interferometry: The application of Kalman filtering to the analysis of very long baseline interferometry data, *J. Geophys. Res.*, *95*, 12,561–12,581, 1990.

Lichten, S.M., Estimation and filtering for high-precision GPS positioning applications, *Manuscr. Geod.*, *15*, 159–176, 1990.

Niell, A. E., Global mapping functions for the atmosphere delay at radio wavelengths, *J. Geophys. Res.*, *101*, *NO. B2*, 3227–3246, 1996.

Resch, G. M., Water vapor radiometry in geodetic applications, *Geodetic Refraction*, F. K. Brunner (ed.), Springer-Verlag, New York, 1984.

Schupler, B. R., Allshouse, R. L., and Clark, T. A., Signal characteristics of GPS user antennas, *Navigation*, *41*, 277–295, 1994.

Webb, F. H. and J. F. Zumberge, An Introduction to the GIPSY/OASIS-II, *JPL Publ.*, *D-11088*, 1993.